Thin Solid Films 593 (2015) 144–149

Contents lists available at ScienceDirect

Thin Solid Films

journal homepage: www.elsevier.com/locate/tsf

Ellipsometry study on Pd thin film grown by atomic layer deposition with Maxwell–Garnett effective medium approximation model

Yihang Zhang [a,b], Xueqi Zhou [a,b], Kun Cao [a,b], Xiuguo Chen [a], Zhang Deng [a], Shiyuan Liu [a,*], Bin Shan [b], Rong Chen [a,c,**]

[a] State Key Laboratory of Digital of Manufacturing Equipment and Technology, School of Mechanical Science and Engineering, Huazhong University of Science and Technology, Wuhan 430074, China
[b] State Key Laboratory of Materials Processing and Die & Mould Technology, School of Materials Science and Engineering, Huazhong University of Science and Technology, Wuhan 430074, China
[c] School of Optical and Electronic Information, Huazhong University of Science and Technology, Wuhan 430074, China

ARTICLE INFO

Article history:
Received 25 June 2015
Received in revised form 10 September 2015
Accepted 24 September 2015
Available online 28 September 2015

Keywords:
Spectroscopic ellipsometry
Pd thin film
General oscillator
Maxwell–Garnett effective medium approximation
Filling medium

ABSTRACT

Maxwell–Garnett effective medium approximation (MG-EMA) model is chosen to study Pd ultrathin film grown on Si substrate, as well as its growth on self-assembled monolayers (SAMs) modified substrate respectively. The general oscillator (GO) model with one Drude and two Lorentz oscillators is firstly applied to fix the optical constants of Pd. Compared with Pd bulk model, MG-EMA model with GO is more reliable to predict the film thickness verified by X-ray reflection test. The stable growth rate on Si substrate reveals our methods are feasible and the quartz crystal microbalance measurement confirms the stability of the ALD chamber. For Pd coverage, MG-EMA fitting result is similar to the statistical computation from scanning electron microscope when Pd ALD cycles are over 400, while large bias exists for cycles under 400, might be due to that air is not the proper filling medium between nanoparticles. Then we change the filling medium into SAMs as a comparison, better fitting performance is obtained. It is demonstrated that the filling medium between nanoparticles is important for the application of MG-EMA model.

1. Introduction

In recent decades, ultrathin noble metal films have attracted lots of attentions in fuel cell catalysts, hydrogen storage, emission control, *etc.* [1–5] In order to achieve a better performance, the focus is on the control of its film thickness and coverage of nanoparticles (NPs). [6,7] Various synthesis methods have been developed such as wet synthesis, chemical vapor deposition and physical vapor deposition. Among these synthesis methods, atomic layer deposition (ALD) is a powerful one to fabricate ultrathin films with great precision [8], achieved through the constant amount of precursors deposited cycle by cycle. Due to its self-limiting and low limit of deposition temperature properties [9,10], a large variety of thin film structures with high conformity and uniformity can be fabricated [11–13]. However, at different growth stages, the film structures and properties are quite unique and independent. Ultrathin film does not form continuous surface coverage but island-like structures. [14,15] The measurement of these noble metal films is important to both understand the initial growth behavior and guide the film fabrication process.

Spectroscopic ellipsometry is a fast and non-destructive thin film characterization technique with atomic sensitivity [16] in comparison with transmission electron microscope and scanning electron microscope (SEM). It is effective in probing various film properties including film thickness, crystallinity, average nanocrystal size, chemical composition, surface roughness, optical and dielectric constants, and optical band gap. [17] Spectroscopic ellipsometry could be used under *ex-situ* mode for the measurement [18] or combined with proper ALD chambers for real time monitoring [19], followed by model selection and data analysis. In earlier study, bulk metal model is a simple original model and has been applied by G.W. Graham [20] to test a very thick Pd film near 1 μm during catalytic reaction with Pd bulk optical constant. Mostly the optical constants of the bulk noble metals can be found in literature [21] and Palik's books [22], however they differ greatly from those of thin film in island growth mode and bulk metal model could not correlate with such structures. Similar structures, such as Au and Ag [23–25], have been simulated with Maxwell–Garnett effective medium approximation (MG-EMA) model to study the optical properties, showing the model matching well with the noble metals properties. MG-EMA describes the material as a kind of compound structure which consists of several different composites and works well for non-ideal film, such as rough surface, interface region and porous structure, considering the medium composed of a host medium with spherical or in a more general case ellipsoidal [26]. Up to date, only few reports [27–29] have been made on the measurement of Pd thin

* Corresponding author.
** Correspondence to: R. Chen, State Key Laboratory of Digital of Manufacturing Equipment and Technology, School of Mechanical Science and Engineering, Huazhong University of Science and Technology, Wuhan 430074, China.
E-mail addresses: shyliu@hust.edu.cn (S. Liu), rongchen@mail.hust.edu.cn (R. Chen).

http://dx.doi.org/10.1016/j.tsf.2015.09.056
0040-6090/

film, while Pd is advantageous over other noble metals in consideration of the cost. So we choose MG-EMA model with general oscillator (GO) to study the size and volume fraction of Pd thin film.

In this study, MG-EMA model has been chosen to study Pd thin film grown on Si substrate, as well as its growth on a self-assembled monolayers (SAMs) modified substrate respectively. We first use GO model with one Drude and two Lorentz oscillators to fix the optical constants of Pd. Quartz crystal microbalance (QCM) measurement is taken to confirm the feasibility and the growth condition of our methods. Compared with Pd bulk model, MG-EMA model with GO is more reliable to predict the film thickness verified by X-ray reflection (XRR) test. For Pd coverage on Si substrate, MG-EMA gives better fitting performance when Pd ALD cycles is over 400, while large bias exists at lower Pd ALD cycles. SAMs have been reported to be effective in adjusting the growth of noble metal thin films [30–33]. Then we choose Pd thin films on SAMs modified substrate as the following research target under the assumption that the filling medium is important for MG-EMA model.

2. Experimental details

2.1. Thin films preparation

Pd films were grown in a bottom heated reactor system at 200 °C. The precursors were Pd(II) hexafluoroacetylacetonate ($Pd(hfac)_2$, Sigma–Aldrich, 97%) and formalin (37% formaldehyde in water with 15% methanol as stabilizer). The reaction pressure maintained at 130 Pa with nitrogen (99.999%) gas continuously passing through the chamber at 100 sccm. The $Pd(hfac)_2$ was sealed in a stainless steel bottle heated to 50 °C. Formalin was kept at room temperature. All the lines were kept at 100 °C to avoid condensation.

Pd ALD experiment was performed by alternatively pulse $Pd(hfac)_2$ and formalin. The ALD time sequences could be expressed as t_1–t_2–t_3–t_4 where t_1 was the pulse time of $Pd(hfac)_2$, t_3 was the pulse time of formalin, t_2 and t_4 represented the N_2 purge time. In our experiments, the time sequence was 2–8–2–8 s. As for the Pd thin films grown on SAMs modified samples, the SAMs were fabricated by octadecyltrichlorosilane ($C_{18}H_{37}SiC_{13}$, ODTS) in a dry, nitrogen atmosphere glovebox, which inhibited the growth of Pd. The growth time of SAMs ranged from 5 min to 24 h and then followed by the Pd ALD experiment, of which the experimental conditions were as mentioned before.

2.2. Measurements

The cross-section and top-section of the Pd film on silicon substrate was examined with a field emission scanning electron microscope (FE-SEM, JSM-7600). Commercial ImageJ 1.46 was utilized to analyze the particle diameter and Pd coverage.

The XRR characterization was performed on a PANalytical B.V. Empyrean X-ray diffractometer with Cu Kα radiation with λ = 1.5406 Å at an incident angle ranging from 0.201° to 1.5°, and the step size was 0.003°.

QCM measurements were made with an INFICON Q-pod monitor in the ALD reaction chamber. The quartz crystal was first deposited with 3 nm Al_2O_3, then the Pd ALD deposition was performed by alternative pulse of $Pd(hfac)_2$ and formalin with a time sequence of 2–8–2–8 s at 200 °C.

Configuration and measurements of both *in-situ* and *ex-situ* mode were performed with J.A. Woollam M2000 Spectroscopic Ellipsometer in reflection mode. *Ex-situ* test were performed on freshly prepared samples. For *in-situ* test, ellipsometry measurements were made before and after every several ALD cycles in sequence. All measurements were made at an incident angle of 68° and the spectral range was 0.75–5 eV. During the experiment, the samples should be carefully held to be flat and steady. The mean square error (MSE) was an unbiased indicator of the goodness of fitting result, with lower values indicating better fits [34].

$$\mathrm{MSE} = \sqrt{\frac{1}{2N-M}\sum_{i=1}^{N}\left[\left(\frac{\psi_i^{\mathrm{mod}}-\psi_i^{\mathrm{exp}}}{\sigma_{\psi,i}^{\mathrm{exp}}}\right)^2+\left(\frac{\Delta_i^{\mathrm{mod}}-\Delta_i^{\mathrm{exp}}}{\sigma_{\Delta,i}^{\mathrm{exp}}}\right)^2\right]} \quad (1)$$

Where N was the number of spectral points, M was the number of fitting parameters. (ψ^{exp}, Δ^{exp}) and (ψ^{mod}, Δ^{mod}) were the measured and calculated ellipsometric angles, respectively, while σ_ψ and σ_Δ were the estimated standard deviations of the measured ellipsometric angles. Generally the fitting result was acceptable when the value of MSE was less than 10.

3. Results and discussion

3.1. Parameterization with GO model

The GO model was a combination of several general oscillators in different types, such as Drude and Lorentz oscillators. For more details, we chose a Pd film specimen as a reference, of which the SEM figure was shown in Fig. 1(a) with thickness about 42 nm. Dielectric function of Pd thin film was parameterized with the combination of one Drude oscillator and two Lorentz oscillators as addressed in Fig. 1(a), where two Lorentz oscillators stayed at the head and tail of the ε_2 curve respectively. Where the Drude oscillator was applied for the intraband transitions caused by free electrons, Lorentz oscillator was for the interband transitions caused by bound electrons which could be commonly found in noble metals [35]. Then the dielectric function of Pd thin film can be described as follows [36]:

$$\tilde{\varepsilon}(E) = \varepsilon_1 + i\varepsilon_2 = 1 - \frac{E_p^2}{E^2 + iE\hbar\Gamma_D} + \sum_{j=1}^{2}\frac{A_j E_{0j}^2}{E_{0j}^2 - E^2 - iE\hbar\gamma_j} + \varepsilon_\infty \quad (2)$$

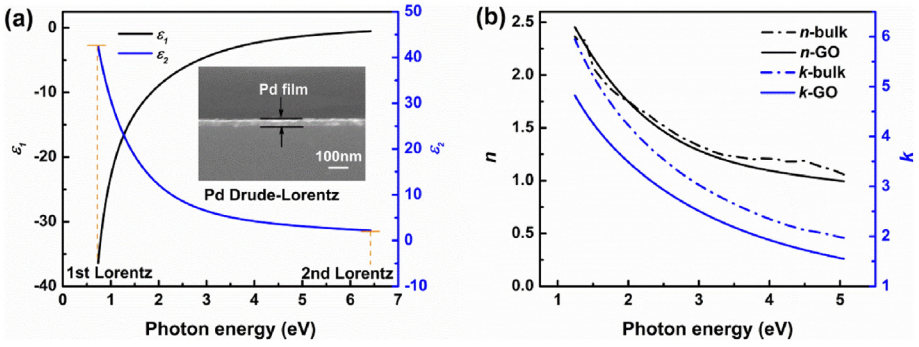

Fig. 1. (a) Spectra of the real (ε_1) and imaginary (ε_2) part of dielectric function of the Pd film specimen (inserted was the SEM image) fitted through GO Pd model with one Drude and two Lorentz oscillators. (b) Comparison of refractive index (n) and extinction coefficient (k) between GO Pd model with a Pd film specimen and bulk Pd model from literature [22].

Table 1
The fitting data with different models and optical constants.

Model/optical constant	d(Å)	(1-f_a)(%)	n@1.96 eV	k@1.96 eV	MSE
Pd/Pd bulk	290.38	–	1.76883	4.28986	12.871
MG-EMA/Pd bulk	350.74	66.2	1.36324	3.15361	9.431
GO/Pd film specimen	407.77	–	1.76032	3.5724	3.108
MG-EMA/Pd film specimen	419.31	94.7	1.69744	3.4171	2.832

d is the thickness of Pd layer; (1-f_a) is the Pd coverage; n is the refractive index; k is the extinction coefficient.

Where the first two terms represented Drude oscillator and the third term was a sum of two Lorentz oscillators, ε_∞ was the dielectric function at high frequencies, E was the photon energy expressed in electron-volts, E_p was the plasmon energy, Γ_D was the damping coefficient; A_j, γ_j and E_{0j} were amplitudes, damping coefficient, oscillations energy of the two Lorentz oscillators respectively.

For additional analysis, the positions for the Lorentz oscillators we applied here did not match well with those reported in references [36,37]. However it needed to be clarified here that the Lorentz oscillators were used as poles in the fitting process and were intended to ensure the Kramers–Kronig relation rather than to simulate the real interband transition.

Then the bulk model with Pd bulk optical constant (Pd/Pd bulk) was used to evaluate the Pd film specimen. As shown in the first column of Table 1, the fitting result had a deviation of about 31% from the measurement of SEM. Then we changed the model into GO Pd model with the optical constant obtained from the Pd film specimen (GO/Pd film specimen) for the following fitting process. The thickness obtained from the GO model correlated well with that of SEM measurement; meanwhile the MSE was smaller compared to the bulk model. It verified the difference of optical properties between bulk Pd and Pd thin film.

Generally the optical constants of the thin film were different from those of optically thick films and that of bulk. [38] Fig. 1(b) exhibited the curves of optical constants, showing the extinction coefficient (k) of our GO Pd model with a Pd film specimen was smaller than that of bulk Pd model from P.B. Johnson and R.W. Christy collected in Palik's book [22]. This might be due to diminished conductivity of the island film if not interrupted completely by the partition of the metal film layer into disconnected islands. [39] In contrast, the refractive index (n) was nearly the same with that of bulk Pd.

Through the GO Pd model, the growth of Pd thin film could be analyzed in both *in-situ* and *ex-situ* modes. As shown in Fig. 2(a), the subtle changes were measured through *in-situ* mode shown in the inserted top-right corner. To make more accurate fitting, multi-sample analysis has been employed with unique model. In this analysis, the dielectric function was determined from several ellipsometric spectra obtained for samples with different film thicknesses [16]. The fitting results verified the stability of our chamber and provided extra information of void content change. The growth rate per cycle (GPC) for *in-situ* mode was relatively stable and small and it stayed at around 0.031 Å/cycle, with the rate of thickness gain per cycle increased at around 100 cycles. The *in-situ* results revealed that our methods were feasible and could be applied to testify our future experiments. So the *ex-situ* experiments were performed afterwards, resulting in a GPC of 0.07 Å/cycle derived from the black line from Fig. 2(a).

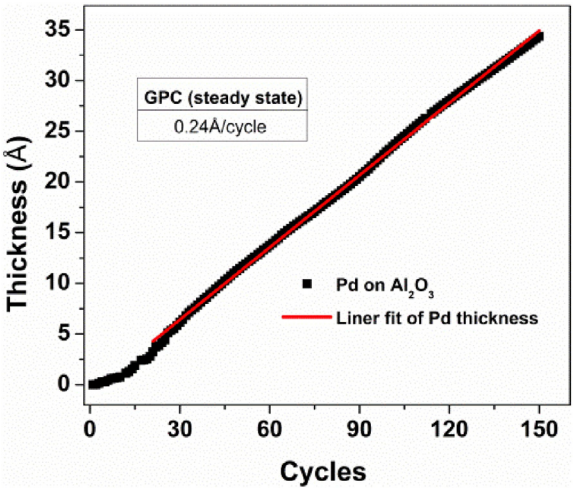

Fig. 3. QCM measurement of Pd ALD grown on Al_2O_3.

The stability of our Pd ALD process was further tested with QCM measurement of Pd grown on Al_2O_3 substrate shown in Fig. 3. At nucleation stage, the growth rate slowly increased and reached a steady state after 30 cycles with a stable GPC of 0.24 Å/cycle, which was similar to the reported value. [40].

3.2. MG-EMA model fitting analysis

To get more details from the SE data including Pd coverage and to approach the real state of thin film, our GO model was converted into MG-EMA model. The Pd thin film growth on Si substrate was schematically shown in Fig. 4(a) and the MG-EMA layer included two kinds of composites, void and GO/Pd. Assuming the inclusion particles in spherical shape, MG-EMA model for two components can be expressed as: [41]

$$\frac{\varepsilon_{MG}-\varepsilon_b}{\varepsilon_{MG}+2\varepsilon_b} = f_a \frac{\varepsilon_a-\varepsilon_b}{\varepsilon_a+2\varepsilon_b} \tag{3}$$

Where ε_{MG} was the effective dielectric function of the mixture, ε_b was the dielectric function of the host material (in our case Pd), ε_a was the dielectric function of the guest material (in our case void or SAMs), f_a was the volume fraction of the guest material, and (1- f_a) was the Pd coverage.

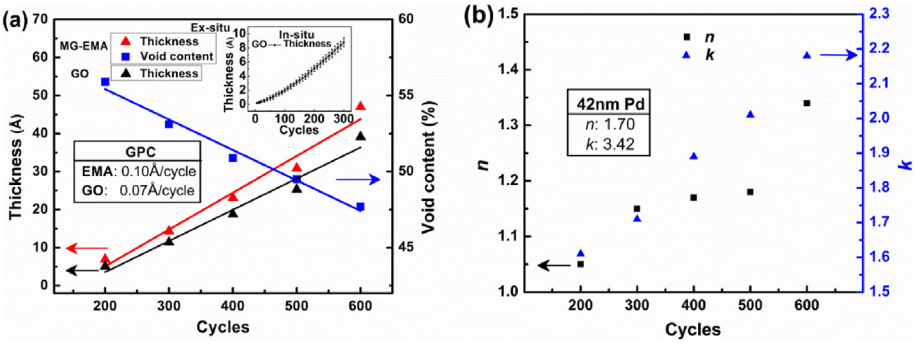

Fig. 2. (a) Thickness and void content change for *ex-situ* and *in-situ* (inserted top-right) grown Pd thin film samples on Si substrate with MG-EMA and GO model respectively. (b) Change of refractive index (n) and extinction coefficient (k) with MG-EMA model.

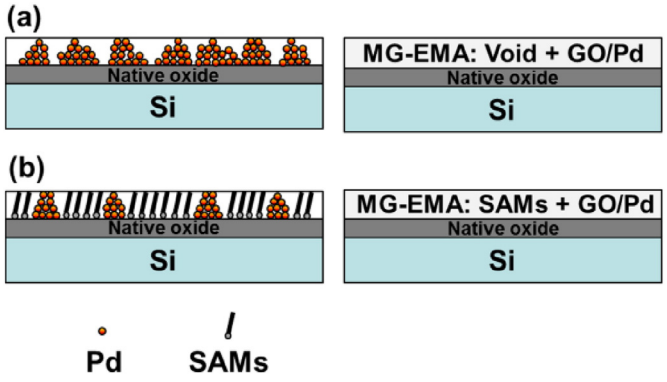

Fig. 4. The schematic of Pd thin film growth morphology and layer model structure used for fitting on (a) Si substrate (b) SAMs modified substrate.

We could see in the second and fourth column of Table 1, the MSE was declining as the model changed, revealing a better fitting performance for MG-EMA model, while the large Pd coverage showed that the film had been almost continuous. The *ex-situ* sample fitting results were shown in Fig. 2(a), the GPC fitted with MG-EMA model was 0.10 Å/cycle, close to that with GO model. For the void content in MG-EMA model, it decreased from 55.9% at 200 cycles to 47.7% at 600 cycles. The change of n and k was in accordance with the trend of thickness as shown in Fig. 2(b); values of n and k became larger as the cycles increased, and gradually got closer to those of 42 nm Pd specimen.

XRR test was performed as a reference to evaluate our model fitting results. As shown in Fig. 5, obvious interference fringes could be observed in the XRR curves. The intensity of the X-ray reflectivity dropped abruptly at a critical angle α_c. When incident angle was below α_c, the X-ray gave a total reflection on the film while otherwise the interference happened. Based on the distance between each peaks, the film thickness could be obtained from the equation below:

$$t = \frac{\lambda/2}{\sqrt{\alpha_{m+1}^2 - \alpha_c^2} - \sqrt{\alpha_m^2 - \alpha_c^2}} \tag{4}$$

Where t was the film thickness, λ was the wavelength of X-ray, α_c was the critical angle as shown by the arrows in Fig. 5. And α_{m+1}, α_m were the $(m+1)$th and mth fringes respectively.

From the comparison of the thickness in Fig. 5, the fitting results matched well with the XRR data. A small deviation existed, which could be attributed to interfacial roughness, only taken into account in X-ray modeling. [42].

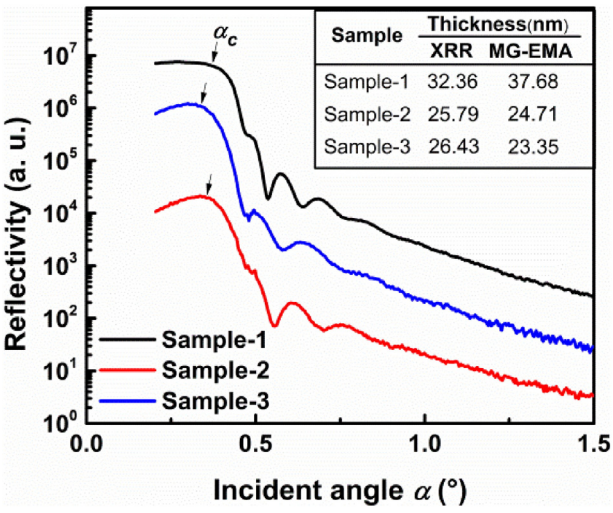

Fig. 5. The XRR curves for Pd thin films on Si substrate and the comparison of the film thickness between XRR measurement and MG-EMA model fitting results.

From Fig. 6, we could see that with the cycles increasing, at early film-formed stage, the Pd NPs existed and immigrated thus the surface void decreased and the NP size almost linearly increased with a growth rate of 0.35 Å/cycle. To further study the growth of Pd NPs, we compared the SEM data with MG-EMA data, as shown in Fig. 7(a). The trend of the Pd coverage indicated by MG-EMA was similar with that of SEM, but the value was about 5.4–25.9% larger than that of SEM. We could see that from 200 to 400 cycles, the bias was quite large; afterward for 400 cycles above, MG-EMA was capable of fitting well. However for 200 to 400 cycles, the existence of large void proportion made MG-EMA not an appropriate approach, which was stated that the MG-EMA should be restricted to small filling factors [43] and the volume filling fraction of the inclusions should be smaller than the value for which the percolation limit occurs (~0.4) [26]. The Pd NP average size could be obtained as well, while the ratio to the thickness decreased as the cycles gained and stayed at around 5 over 400 cycles. It implied that maybe the shape of NPs was critical for the fitting. Some studies pointed out larger particles dominated the optical response of metal NPs [44]. While at early cycles, size of these NPs was quite smaller resulting in a larger fitting deviation. That means for early cycles, we needed to derive a different model or modify our MG-EMA. The medium between NPs was perhaps the main factor that influenced the fitting performance, of which air was not the proper one. Some studies focused on the noble metal NPs grown in polymers such as Ag NPs in fluoropolymer [24], Ag NPs in polystyrene matrix [23], Au NPs in polystyrene [45]. It demonstrated that polymer filling could give a distinct influence of the NPs optical properties. Based on this point, therefore we took SAMs instead as the filling medium for the following test.

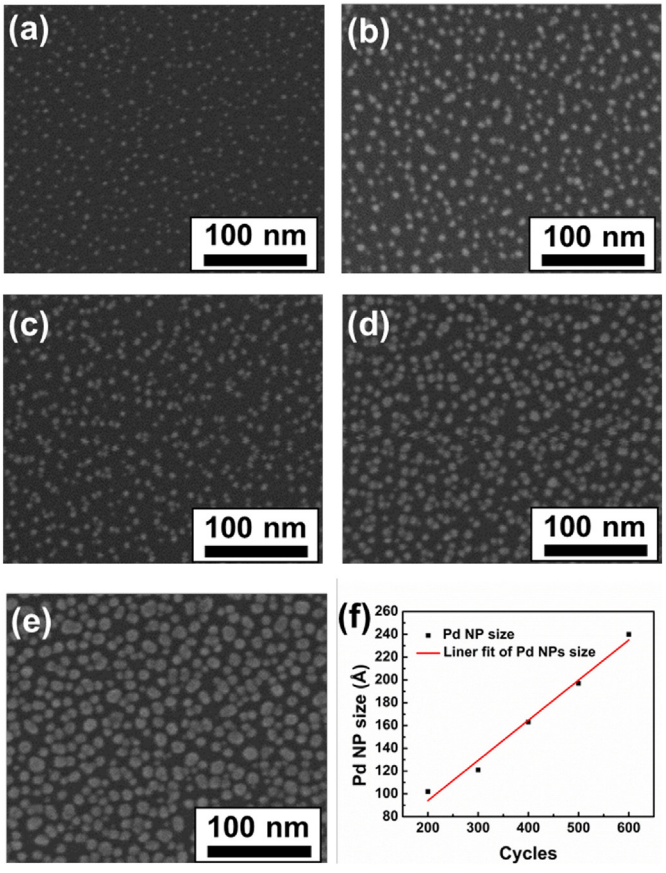

Fig. 6. SEM images of Pd thin film samples on Si substrate with different Pd ALD cycles (a) 200 cycles (b) 300 cycles and (c) 400 cycles (d) 500 cycles (e) 600 cycles and (f) Pd NP size statistically measured from SEM images as a function of Pd ALD cycles.

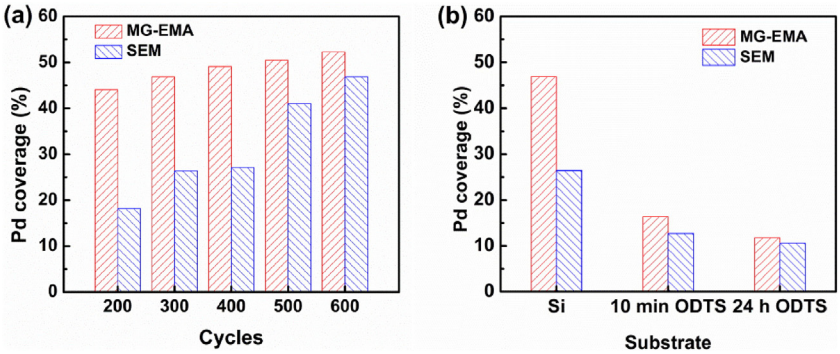

Fig. 7. Comparison of Pd coverage between MG-EMA model fitting results and SEM measurement for (a) Pd thin films on Si substrate with different Pd ALD cycles (b) Pd thin films on different substrates (Si, 10 min ODTS, 24 h ODTS) with 300 Pd ALD cycles.

To further verify our MG-EMA on Pd thin films at lower void content, the fitting data of Pd thin films on SAMs modified substrate were studied. From SEM images in Fig. 8, we could find a more uniform and well-dispersed structure. Spectroscopic ellipsometry test was taken on initial SAMs modified Si substrate and a Cauchy model was applied to fit the SAMs component, with varied values of A. Then we maintained the optical constants of the SAMs component. After the Pd deposition, then the MG-EMA model was used to characterize the Pd thin film on SAMs modified substrate and the schematic was shown in Fig. 4(b). The first layer was silicon substrate, followed by the MG-EMA layer which consisted of SAMs (Cauchy model) and GO Pd. Then fitting the data, we could derive the film thickness and the Pd coverage from the MG-EMA model. Cauchy model could be expressed as follows [17]:

$$n = A + \frac{B}{\lambda^2} + \frac{C}{\lambda^4} \tag{5}$$

Where A, B and C were constants fitted in the modeling.

We could find that the data of Pd thin films on SAMs substrate were in accordance with the SEM data from Fig. 7(b), which showed that MG-EMA was a good candidate in fitting Pd grown in polymers. The comparison of Pd thin films between the substrates of Si and SAMs (ODTS) in different growth time was made at smaller 300 Pd ALD cycles. As the ODTS growth time increased, the NPs could be more isolated and well dispersed, and the fitting deviation could be quite smaller within 5% which was much less than the fitting of Pd thin film on Si substrate. ODTS had a strong blocking effect and at 10 min growth the blocking effect could almost be maximized, while at 24 h growth, the Pd coverage decreased slightly which produced a smaller deviation from model fitting. This was due to a more universal distribution of Pd on SAMs modified substrate, which may be more suitable for the MG-EMA theory. MG-EMA was exact for a geometry where the entire space was filled with coated spheres, each with identical ratio of inner to outer radius, such that one component was the core material (isolated inclusions) and the other was the coating material (the host). [46].

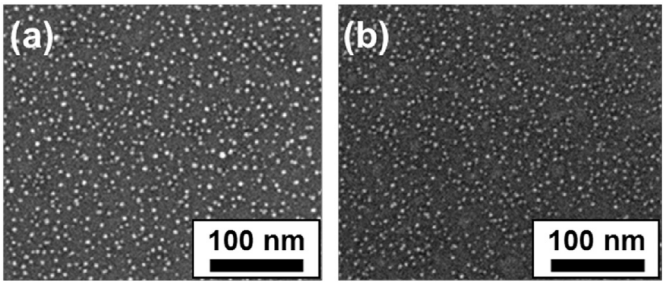

Fig. 8. SEM images of Pd thin films on SAMs of (a) 10 min ODTS and (b) 24 h ODTS modified substrate.

4. Conclusions

In summary, MG-EMA model was used to characterize Pd thin films fabricated by ALD on Si substrate and SAMs modified substrate respectively. Stable growth rate proved the feasibility of our methods and the QCM measurement further confirmed the stability of our ALD chamber. Compared with Pd bulk model, MG-EMA combined with GO model was more reliable to evaluate the film thickness, verified by XRR test. For Si substrate, the fitting result for Pd coverage could match well with SEM only when Pd cycles were over 400. For lower Pd cycles, better fitting results were obtained when we changed the filling medium between NPs from air to SAMs. The type of filling medium was demonstrated important for the application of MG-EMA model.

Acknowledgments

This work is supported by the National Basic Research Program of China (2013CB934800), the National Natural Science Foundation of China (51575217, 51572097, 51475191, and 51405172), the Hubei Province Funds for Distinguished Young Scientists (2015CFA034 and 2014CFA018), Fundamental Research Funds for the Central Universities, HUST (2014TS037), and the National Instrument Development Specific Project of China (Grant No. 2011YQ160002). Rong Chen acknowledges the State Key Laboratory of Digital Manufacturing Equipment and Technology Funding (DMET2015A01), the Thousand Young Talents Plan, the Recruitment Program of Global Experts, and Changjiang Scholars and Innovative Research Team in University (No.: IRT13017). The authors also would like to acknowledge HUST Innovation Institute cross disciplinary team on "innovative emission control catalysts and key equipment research", equipment supports from AMETEK lab, and the technical support from the Analytic Testing Center of HUST.

References

[1] Z. Peng, H. Yang, Synthesis and oxygen reduction electrocatalytic property of Pt-on-Pd bimetallic heteronanostructures, J. Am. Chem. Soc. 131 (2009) 7542–7543.
[2] H. Kobayashi, M. Yamauchi, H. Kitagawa, Y. Kubota, K. Kato, M. Takata, Atomic-level Pd–Pt alloying and largely enhanced hydrogen-storage capacity in bimetallic nanoparticles reconstructed from core/shell structure by a process of hydrogen absorption/desorption, J. Am. Chem. Soc. 132 (2010) 5576–5577.
[3] F. Tao, M.E. Grass, Y. Zhang, D.R. Butcher, J.R. Renzas, Z. Liu, J.Y. Chung, B.S. Mun, M. Salmeron, G.A. Somorjai, Reaction-driven restructuring of Rh–Pd and Pt–Pd core–shell nanoparticles, Science 322 (2008) 932–934.
[4] E. Rikkinen, A. Santasalo-Aarnio, S. Airaksinen, M. Borghei, V. Viitanen, J. Sainio, E.I. Kauppinen, T. Kallio, A.O.I. Krause, Atomic layer deposition preparation of Pd nanoparticles on a porous carbon support for alcohol oxidation, J. Phys. Chem. C 115 (2011) 23,067–23,073.
[5] J. Lu, B. Fu, M.C. Kung, G. Xiao, J.W. Elam, H.H. Kung, P.C. Stair, Coking- and sintering-resistant palladium catalysts achieved through atomic layer deposition, Science 335 (2012) 1205–1208.

[6] T. Schalow, B. Brandt, D.E. Starr, M. Laurin, S.K. Shaikhutdinov, S. Schauermann, J. Libuda, H.-J. Freund, Size-dependent oxidation mechanism of supported Pd nanoparticles, Angew. Chem. Int. Ed. 45 (2006) 3693–3697.
[7] O.M. Wilson, M.R. Knecht, J.C. Garcia-Martinez, R.M. Crooks, Effect of Pd nanoparticle size on the catalytic hydrogenation of allyl alcohol, J. Am. Chem. Soc. 128 (2006) 4510–4511.
[8] H. Feng, J. Lu, P.C. Stair, J.W. Elam, Alumina over-coating on Pd nanoparticle catalysts by atomic layer deposition: enhanced stability and reactivity, Catal. Lett. 141 (2011) 512–517.
[9] S.T. Christensen, J.W. Elam, Atomic layer deposition of Ir–Pt alloy films, Chem. Mater. 22 (2010) 2517–2525.
[10] G.A. Ten Eyck, S. Pimanpang, J.S. Juneja, H. Bakhru, T.-M. Lu, G.-C. Wang, Plasma-enhanced atomic layer deposition of palladium on a polymer substrate, Chem. Vap. Depos. 13 (2007) 307–311.
[11] J.S. Becker, S. Suh, S. Wang, R.G. Gordon, Highly conformal thin films of tungsten nitride prepared by atomic layer deposition from a novel precursor, Chem. Mater. 15 (2003) 2969–2976.
[12] J.S. Jur, J.C. Spagnola, K. Lee, B. Gong, Q. Peng, G.N. Parsons, Temperature-dependent subsurface growth during atomic layer deposition on polypropylene and cellulose fibers, Langmuir 26 (2010) 8239–8244.
[13] D.M. Hausmann, P. de Rouffignac, A. Smith, R. Gordon, D. Monsma, Highly conformal atomic layer deposition of tantalum oxide using alkylamide precursors, Thin Solid Films 443 (2003) 1–4.
[14] D.N. Goldstein, S.M. George, Enhancing the nucleation of palladium atomic layer deposition on Al_2O_3 using trimethylaluminum to prevent surface poisoning by reaction products, Appl. Phys. Lett. 95 (2009) 143,106.
[15] H. Feng, J.W. Elam, J.A. Libera, W. Setthapun, P.C. Stair, Palladium catalysts synthesized by atomic layer deposition for methanol decomposition, Chem. Mater. 22 (2010) 3133–3142.
[16] H. Fujiwara, Spectroscopic Ellipsometry: Principles and Applications, Wiley, West Sussex, UK, 2007.
[17] H.G. Tompkins, E.A. Irene, Handbook of Ellipsometry, William Andrew, New York, 2005.
[18] S. Liu, X. Chen, C. Zhang, Development of a broadband Mueller matrix ellipsometer as a powerful tool for nanostructure metrology, Thin Solid Films 584 (2015) 176–185.
[19] E. Langereis, S.B.S Heil, H.C.M. Knoops, W. Keuning, M.C.M. van de Sanden, W.M.M. Kessels, *In-situ* spectroscopic ellipsometry as a versatile tool for studying atomic layer deposition, J. Phys. D. Appl. Phys. 42 (2009) 073,001.
[20] G.W. Graham, D. König, B.D. Poindexter, J.T. Remillard, W.H. Weber, Ellipsometric study of a palladium catalyst during the oxidation of carbon monoxide and methane, Top. Catal. 8 (1999) 35–43.
[21] P.B. Johnson, R.W. Christy, Optical constants of the noble metals, Phys. Rev. B 6 (1972) 4370–4379.
[22] E.D. Palik, Handbook of Optical Constants of Solids, Academic Press, UK, 1985.
[23] T.W.H. Oates, Real time spectroscopic ellipsometry of nanoparticle growth, Appl. Phys. Lett. 88 (2006) 213,115.
[24] K.C. See, J.B. Spicer, J. Brupbacher, D. Zhang, T.G. Vargo, Modeling interband transitions in silver nanoparticle–fluoropolymer composites, J. Phys. Chem. B 109 (2005) 2693–2698.
[25] T. Ung, L.M. Liz-Marzan, P. Mulvaney, Optical properties of thin films of $Au@SiO_2$ particles, J. Phys. Chem. B 105 (2001) 3441–3452.
[26] R.W. Cohen, G.D. Cody, M.D. Coutts, B. Abeles, Optical properties of granular silver and gold films, Phys. Rev. B 8 (1973) 3689–3701.
[27] Y. Yamada, K. Tajima, S. Bao, M. Okada, K. Yoshimura, Hydrogenation and dehydrogenation processes of palladium thin films measured *in-situ* by spectroscopic ellipsometry, Sol. Energy Mater. Sol. Cells 93 (2009) 2143–2147.
[28] A.A. Wronkowska, A. Wronkowski, A. Bukaluk, M. Trzciński, K. Okulewicz, Characterization of In/Pd and Pd/In/Pd thin films by ellipsometric, XRD and AES methods, Appl. Surf. Sci. 253 (2007) 3367–3371.
[29] G.K. Mor, L.K. Malhotra, D. Bhattacharyya, Effect of palladium cap layer thickness on desorption of hydrogen from PrH_x films: a spectroscopic ellipsometry study, J. Appl. Phys. 90 (2001) 1795–1800.
[30] A. Rezaee, K.K.H. Wong, T. Manifar, S. Mittler, Octadecyltrichlorosilane (OTS): a resist for OMCVD gold nanoparticle growth, Surf. Interface Anal. 41 (2009) 615–623.
[31] K. Cao, Q. Zhu, B. Shan, R. Chen, Controlled synthesis of Pd/Pt core shell nanoparticles using area-selective atomic layer deposition, Sci. Rep. 5 (2015) 8470.
[32] R. Chen, S.F. Bent, Chemistry for positive pattern transfer using area-selective atomic layer deposition, Adv. Mater. 18 (2006) 1086–1090.
[33] R. Chen, S.F. Bent, Highly stable monolayer resists for atomic layer deposition on germanium and silicon, Chem. Mater. 18 (2006) 3733–3741.
[34] F. Haidu, O.D. Gordan, D.R.T. Zahn, *In situ* ellipsometric study of copper growth on silicon, Thin Solid Films 520 (2012) 4410–4417.
[35] Z. Montiel-González, S.E. Rodil, S. Muhl, A. Mendoza-Galván, L. Rodríguez-Fernández, Amorphous carbon gold nanocomposite thin films: structural and spectro-ellipsometric analysis, Thin Solid Films 519 (2011) 5924–5932.
[36] A.D. Rakić, A.B. Djurišić, J.M. Elazar, M.L. Majewski, Optical properties of metallic films for vertical-cavity optoelectronic devices, Appl. Opt. 37 (1998) 5271–5283.
[37] J.H. Weaver, R.L. Benbow, Low-energy interband adsorption in Pd, Phys. Rev. B 12 (1975) 3509–3510.
[38] C. Liu, J. Erdmann, A. Macrander, *In situ* spectroscopic ellipsometry as a surface-sensitive tool to probe thin film growth, Thin Solid Films 355–356 (1999) 41–48.
[39] A. Röseler, E.-H. Korte, The optical constants of metallic island films as used for surface enhanced infrared absorption, Thin Solid Films 313–314 (1998) 732–736.
[40] J.W. Elam, A. Zinovev, C.Y. Han, H.H. Wang, U. Welp, J.N. Hryn, M.J. Pellin, Atomic layer deposition of palladium films on Al_2O_3 surfaces, Thin Solid Films 515 (2006) 1664–1673.
[41] R.J. Gehr, R.W. Boyd, Optical properties of nanostructured optical materials, Chem. Mater. 8 (1996) 1807–1819.
[42] V. Edon, M.-C. Hugon, B. Agius, O. Durand, C. Eypert, C. Cardinaud, Investigation of lanthanum and hafnium-based dielectric films by X-ray reflectivity, spectroscopic ellipsometry and X-ray photoelectron spectroscopy, Thin Solid Films 516 (2008) 7974–7978.
[43] C.G. Granqvist, O. Hunderi, Optical properties of ultrafine gold particles, Phys. Rev. B 16 (1977) 3513–3534.
[44] U. Kreibig, M. Vollmer, Optical Properties of Metal Clusters, Springer-Verlag Berlin Heidelberg, New York, 1995.
[45] J. Kim, H. Yang, P.F. Green, Tailoring the refractive indices of thin film polymer metallic nanoparticle nanocomposites, Langmuir 28 (2012) 9735–9741.
[46] O. Levy, D. Stroud, Maxwell Garnett theory for mixtures of anisotropic inclusions: application to conducting polymers, Phys. Rev. B 56 (1997) 8035–8046.